



OPEN ACCESS

EDITED BY

Jose Antonio Rodriguez Martin,
Instituto Nacional de Investigación y
Tecnología Agroalimentaria (INIA), Spain

REVIEWED BY

Faisal Hamzah,
National Research and Innovation Agency
(BRIN), Indonesia
Aulia Rahim,
Diponegoro University, Indonesia

*CORRESPONDENCE

Huade Guan

✉ huade.guan@flinders.edu.au

RECEIVED 08 October 2025

REVISED 24 December 2025

ACCEPTED 29 December 2025

PUBLISHED 27 January 2026

CITATION

Yang W, Guan H, Wang J, Abiodun OO,
Zhou Y and Batelaan O (2026) An
anthropogenically induced gradient in net
carbon exchange of a temperate mangrove
forest in South Australia.
Front. Clim. 7:1720464.
doi: 10.3389/fclim.2025.1720464

COPYRIGHT

© 2026 Yang, Guan, Wang, Abiodun, Zhou
and Batelaan. This is an open-access article
distributed under the terms of the [Creative
Commons Attribution License \(CC BY\)](#). The
use, distribution or reproduction in other
forums is permitted, provided the original
author(s) and the copyright owner(s) are
credited and that the original publication in
this journal is cited, in accordance with
accepted academic practice. No use,
distribution or reproduction is permitted
which does not comply with these terms.

An anthropogenically induced gradient in net carbon exchange of a temperate mangrove forest in South Australia

Wenjing Yang¹, Huade Guan^{1*}, Jingfeng Wang²,
Olanrewaju O. Abiodun¹, Yifei Zhou^{1,3} and Okke Batelaan¹

¹National Centre for Groundwater Research and Training, and Ecology Evolution and Environment Section, College of Science and Engineering, Flinders University, Adelaide, SA, Australia, ²School of Civil and Environmental Engineering, Georgia Institute of Technology, Atlanta, GA, United States, ³College of Environment and Ecology, Chongqing University, Chongqing, China

Mangrove forests are one of the most effective carbon assimilation and storage ecosystems, providing crucial ecosystem services in coastal regions. However, they face potential threats from climate change, human activities, as well as their interactive effects, which have not yet been well investigated. In this study, we investigated net ecosystem production (NEP) of a temperate mangrove forest next to salt-production ponds in South Australia. The hypersaline salt ponds next to the land side of the mangrove forest create a salinity gradient in the forest. The study was based on eddy covariance measurement of carbon flux from November 2017 to December 2019, along with a salinity stress index (SSI), a new sea/land breeze index (W_b), and flooded fraction (F). The result shows significant difference in mangrove NEP between seaside and landside sources, which can be attributed to salinity difference and tidal inundation. The negative impact of salinity stress on mangrove NEP can be mitigated by tidal flooding but the tidal flushing effect is limited toward the landside end. Additionally, an optimal temperature range (16–24 °C) is identified, above and below which the NEP rate reduces, and this range is lower than that reported for mangroves in tropical and subtropical areas. The negative impact of high temperature on NEP can be slightly relieved by sea breezes. At this particular mangrove site, sea level rise may enhance salt flushing and thus the carbon sink. The carbon flux data measured in this study provide a baseline before a dieback event in 2020, aiding in assessing losses and informing temperate mangrove management in salinity-affected areas.

KEYWORDS

ecosystem CO₂ exchange, heat stress, salinity stress, sea breezes, temperate mangrove, tidal flooding

1 Introduction

Mangrove forests, known for their high carbon densities (Richards et al., 2020; Li et al., 2024), possess the highest capacity among blue carbon ecosystems for capturing and storing carbon (Song et al., 2023; Gu et al., 2022). They contribute to improving coastal water quality and essential ecosystem services (Montgomery et al., 2019; Narayan et al., 2019; Zhang et al., 2024). However, they are threatened by anthropogenic activities (Cahyaningsih et al., 2022; Sanders et al., 2014; Farzanmanesh et al., 2024) and climate change impacts (Gilman et al., 2008; Jimenez et al., 1985; Sippo et al., 2018), including land use conversion, hydrological alteration, pollution, storms and hurricanes, droughts and heatwaves, and sea level rise (Duke

et al., 2017; Krauss et al., 2014; Maiti and Chowdhury, 2013; Radabaugh et al., 2021; Richards et al., 2020; Smith et al., 2009).

Generally, mangroves are adapted to grow in coastal areas, with a unique ability to tolerate high salinity (Parida and Jha, 2010), which distinguishes mangroves from terrestrial forests. However, increasing salinity levels can diminish forest structure, functions, and productivity (Ahmed et al., 2022; Perri et al., 2023; Castañeda-Moya et al., 2006), potentially leading to canopy loss or mortality in extreme cases, as evidenced by studies documenting mangrove dieback worldwide (Dittmann et al., 2022; Jaramillo et al., 2018; Lovelock et al., 2017; Senger et al., 2021). For example, a dieback event of temperate mangroves (*Avicennia marina*) occurred in South Australia in 2020 (Dittmann et al., 2022), resulting in the loss of approximately 9 hectares of the mangrove forest (Water, 2021). Porewater salinity (>100 ppt) measured during this dieback event was one of the most extreme hypersalinity cases known in mangroves (Dittmann et al., 2022), exceeding the threshold of 68.5 ppt reported for widespread canopy loss in *Avicennia marina* (Lovelock et al., 2017). The dieback was attributed to decommissioned salt production ponds adjacent to the northeast side of the mangrove forest. In fact, the impact of hypersalinity on this mangrove forest occurred before the dieback incident.

Direct monitoring of plant responses to salinity in the field is labor-intensive and time-consuming due to high spatial variability requiring many samples within a small area (Dittmann et al., 2022; Ahmed et al., 2022; Rhoades, 1990; Rhoades et al., 1992). To overcome these difficulties, spectral data have increasingly been used to assess plant biochemical responses to salinity. For example, Stong (2008) proposed an approach using a spectroradiometer to measure field salinity and plant responses. The rapid advancement of remote sensing technology, such as Sentinel data, has enhanced land surface monitoring by providing high-resolution and accurate observations (Jones et al., 2011; Torres et al., 2012). The technology development has provided an opportunity to extend Stong's work to landscapes with larger spatial variability (seaside and landside areas). With the advantage of Sentinel-2 data, it is possible to efficiently map large-scale distributed plant salinity gradients.

Except for hypersaline conditions, another notable difference that marks this mangrove site from other ecotypes is the influence of tidal flooding. Coastal wetlands are highly vulnerable to sea level rise, causing frequent tidal inundation and saltwater intrusion (Dai et al., 2024; Lovelock et al., 2015; Lovelock et al., 2017; Krauss et al., 2008; Li et al., 2020). Tides affect mangrove carbon uptake through several mechanisms (Zhu et al., 2021): prolonged inundation can cause oxygen deficiency in soils (Li et al., 2020; Pezeshki, 2001); thermal contrasts between tidal water and soil can alter physiological conditions; and tidal currents may export nutrients, sediments, and salts, affecting ecosystem balance (Zhu et al., 2021). In most cases, tidal activities increase salinity, which can slow down mangrove growth when seawater is more saline than soil porewater (Ahmed et al., 2022; Gou et al., 2023; Heinsch, 2004). In contrast, the mangrove site in this study has a reversed salinity gradient (50 ppt on the landside and 36 ppt on the seaside observed in October 2018), indicating inland hypersaline conditions (Dittmann et al., 2022). This unusual salinity pattern makes it especially interesting to investigate how tides influence mangrove carbon uptake under contrasting salinity conditions.

In addition to local anthropogenic disturbances, global climate change also affects mangrove ecosystems. Temperature is identified

as a critical factor in mangrove carbon sequestration (Goldstein and Santiago, 2016). Low temperature can reduce metabolic rates, alter membrane permeability, and cause tissue freezing (Duke et al., 1998; Krauss et al., 2008; Ross et al., 2009), while high temperature can lead to enzyme denaturation, membrane damage, and tissue death (Krauss et al., 2008; Lovelock et al., 2016). An optimal temperature range (T_{opt}) of 22 °C–30 °C for most mangrove species has been reported based on leaf-level photosynthetic gas exchange measurements. Mangrove productivity is maximized within this range and decreases outside of it (Duffy et al., 2021; Moore et al., 1973; Noor et al., 2015; Paramita Nandy et al., 2007; Reef et al., 2016). Knowledge of different responses of mangrove carbon sequestration to low- and high-temperatures at the ecosystem scale is necessary for predicting how mangrove forests would perform in the context of global warming.

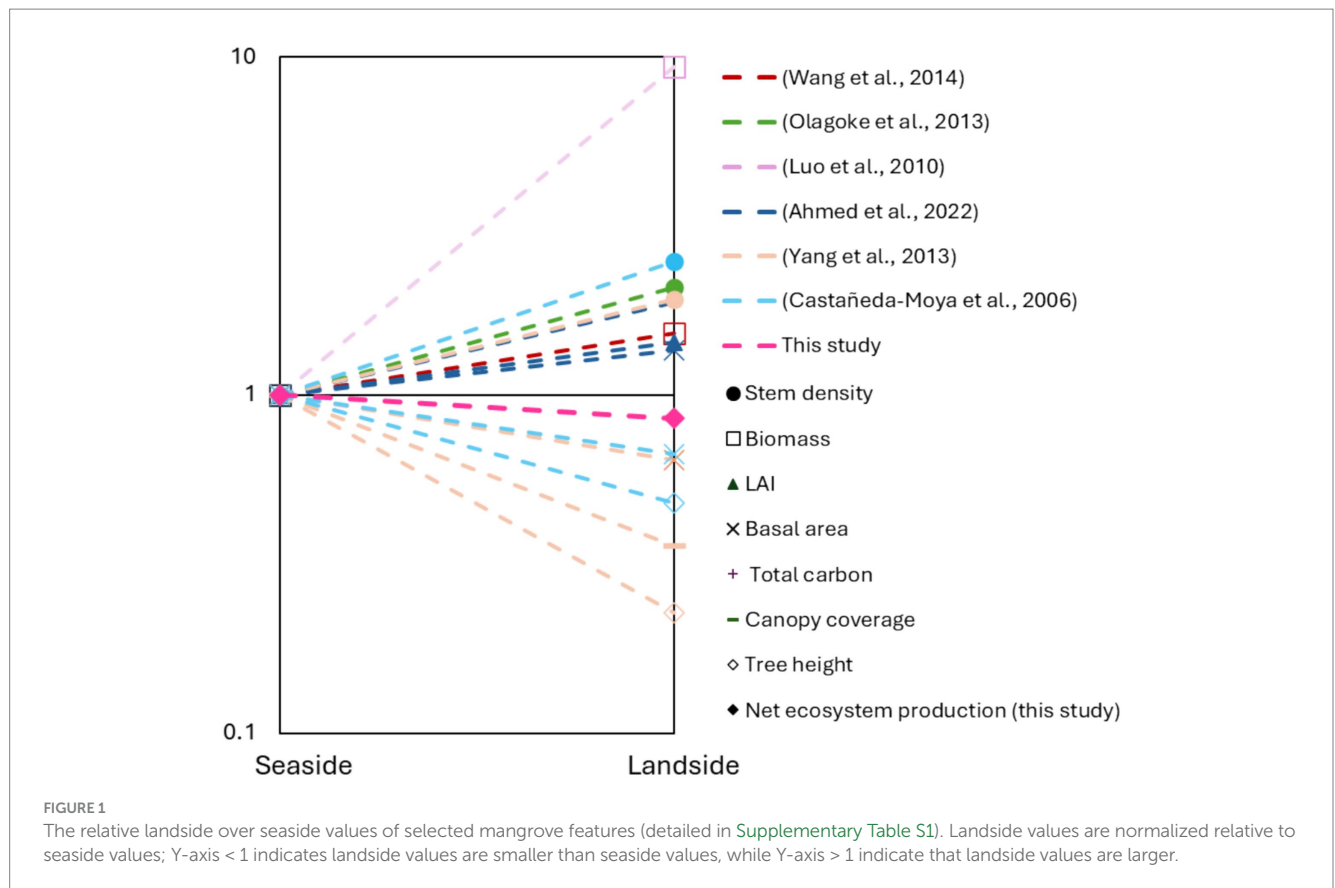
Coastal mangrove forests experience unique land-sea interactions (Zhu et al., 2021). As the land heats up more rapidly than water, sea breezes or onshore winds in coastal regions tend to form during the daytime. Conversely, land breezes or offshore winds typically develop at night or early morning because land cools down more rapidly than water (Miller et al., 2003). Sea breezes bring cool and moist air from the sea (Zhou et al., 2021), indirectly affecting mangrove carbon flux by adjusting the air temperature (cooling effect) and vapor pressure deficit (moistening effect). These cooling and moistening effects would alleviate the stress caused by high temperature, which was usually overlooked in previous studies (Zhu et al., 2021).

The global area of mangrove forests is 145,068 km² in 2020, with approximately 96% located in tropical regions (Jia et al., 2023). Climate change is likely to increase risks to mangrove health in tropical areas (Chung et al., 2023). In contrast, mangrove growth in temperate regions is promoted due to rising temperatures (Morrisey et al., 2010; Saintilan et al., 2014). According to Morrisey et al. (2010), only 1.4% of the global mangrove area is located at latitudes greater than 30°, with 48–55% of these found in southern Australia. However, these temperate mangroves have not been extensively studied. Despite eddy covariance (EC) systems providing continuous monitoring of carbon exchange, EC measurements from temperate mangrove ecosystems are still rare compared to other ecosystems (Alvarado-Barrientos et al., 2021; Gou et al., 2023), partly due to the difficulty in flux tower construction in harsh coastal conditions (e.g., salinity, tides, and a lack of solid foundation).

In summary, EC monitoring sites for temperate mangroves are very rare globally. Although some studies (Supplementary Table S1; Figure 1) have compared forest features in mangrove fringes, interiors, or along transects from the seaward to landward side, ecosystem CO₂ exchange has not been investigated.

Thus, by using eddy covariance measurements the temperate mangrove site in South Australia, we aim to: (1) compare the carbon fluxes between landside and seaside mangroves; (2) assess the effects of salinity stress, tidal flooding, and other meteorological factors on carbon fluxes; (3) evaluate the impact of high temperature stress and sea breezes on mangrove carbon fluxes.

This particular mangrove site faces hypersaline conditions and high temperature risks. As a result, the interactive effects of salinity combined with tidal flooding and high temperature modulated by sea breezes on carbon uptake in temperate mangroves are still poorly understood. The carbon fluxes measured in this study can serve as a baseline to quantify the impact of environmental changes on



mangrove carbon assimilation, e.g., the aforementioned dieback event. The influencing factors investigated here will be useful for predicting the effects of future environmental change on mangrove ecosystem service.

2 Materials and methods

2.1 Study site

The study area is located in a section of gray mangrove forest (*Avicennia marina*) from Barker Inlet to Tourville Bay in Adelaide, South Australia. The forest is bordered by salt marsh, immediately adjacent to hypersaline ponds that were once part of a sea salt production plant. A dieback event, starting in September 2020, caused an approximately 9-hectare loss of the mangrove forest (Water, 2021). This incident is believed to have resulted from hypersaline porewater in the mangrove root zone (Dittmann et al., 2022). The ponds were refilled to operational levels with hypersaline water in December 2019. Before the dieback event, mangrove root zone porewater salinity was 35 ppt at the seaside and 50 ppt at the landside (October 2018). During the dieback event, porewater salinity up to 42 ppt at the seaside and over 100 ppt at the landside (October 2020) was observed (Dittmann et al., 2022).

The forest covers an area of 42 ha, extending a few hundred meters inland from the coastline (Figure 2a). The average vegetation height is 3.7 m, with intermittent inundation depending on tidal flows. The average annual rainfall is 474 mm (1956–2023), mostly in winter (June–August), measured at the

nearby Adelaide Airport, approximately 20 km to the south of the mangrove site. The annual mean air temperature is 16.6 °C (1955–2025). Due to this salinity gradient and tidal inundation, mangrove trees grow to over 5 m at the eastern end and decrease to below 2 m at the western end.

2.2 Workflow and data collection

The research workflow is shown in Figure 3. First, we collected data, including eddy covariance measurements, meteorological, tidal, and satellite data, and we processed data to obtain daytime daily carbon fluxes. Second, key condition indexes, including flooded fraction (*F*), sea/land breezes index (*W_b*), and salinity stress index (SSI), were calculated using hydrometeorological, topographic and remote sensing data. Third, daytime daily carbon flux was separated into landside and seaside groups. Statistical analyses were then conducted to quantify the response of carbon flux to salinity, wind, and tidal flooding conditions under high and low temperature condition.

2.2.1 Eddy covariance measurement

An eddy covariance (EC) tower was set up above the canopy on the St Kilda Mangrove Trail (34°44'47.07744"S, 138°32'15.90072"E), as shown in Figure 2b, to measure the net ecosystem CO₂ exchange (NEE) and meteorological variables, including wind speed and direction (*W_d*), air temperature (*T_a*), and relative humidity (RH). Vapor pressure deficit (VPD) was calculated from *T_a* and RH. The EC system comprised the analyser interface unit, the gas analyser,

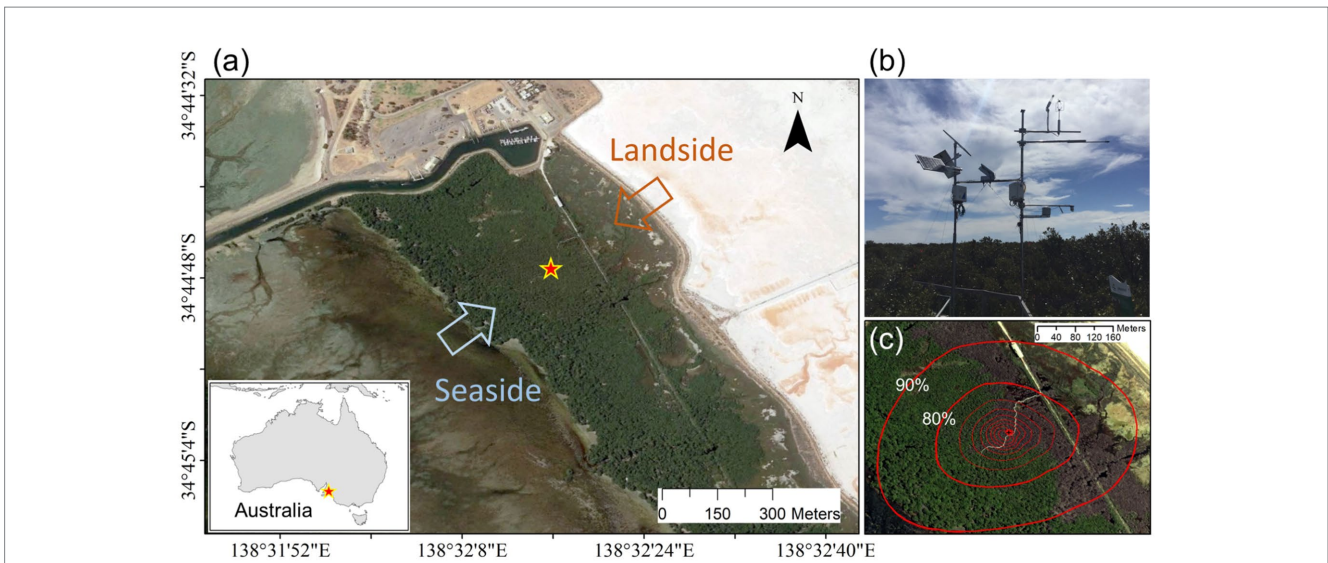


FIGURE 2 Site location (a), observation equipment (b), and flux footprint climatology (c) for the mangrove forest. The red star in (a) marks the location of the flux tower shown in (b). The white area on the top-right of (a) is hypersaline ponds, which is the source of hypersaline porewater of nearby mangrove root zone (landside). The red circles in (c) show the percentage of measured flux originating from the area within each circle.

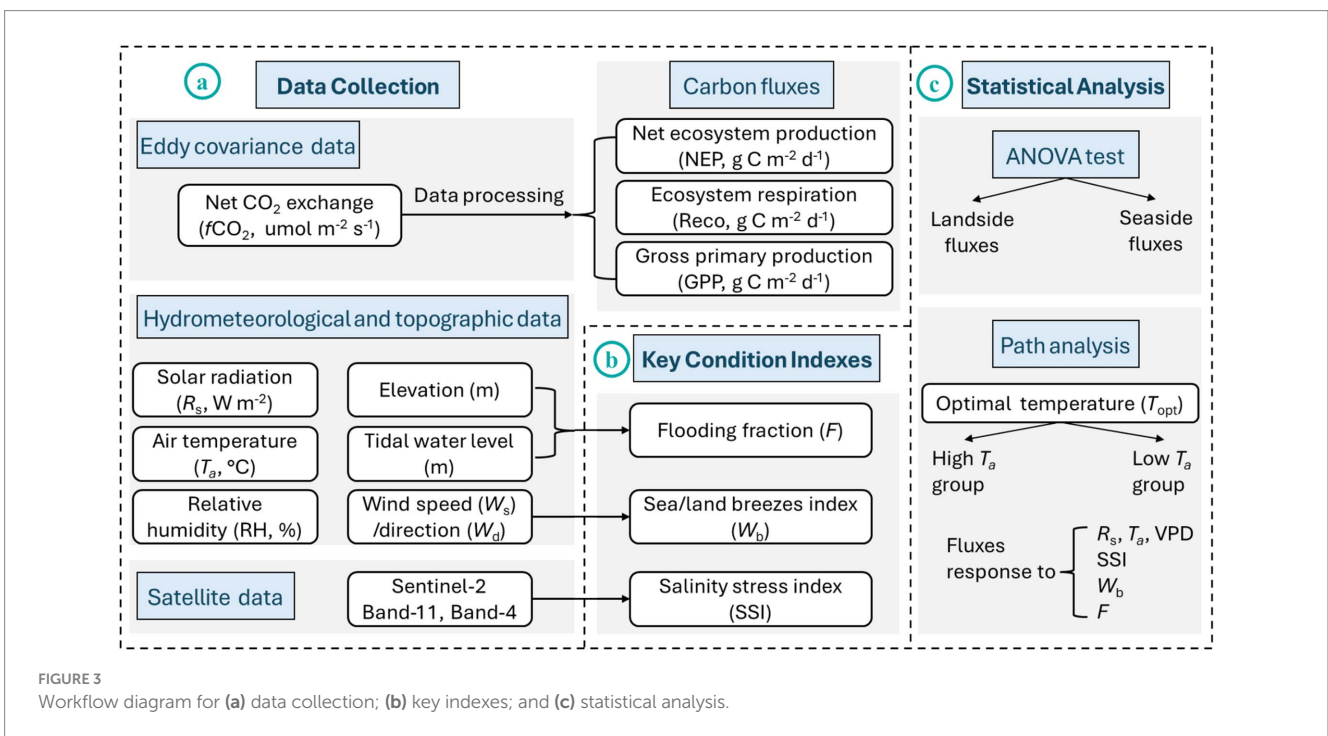


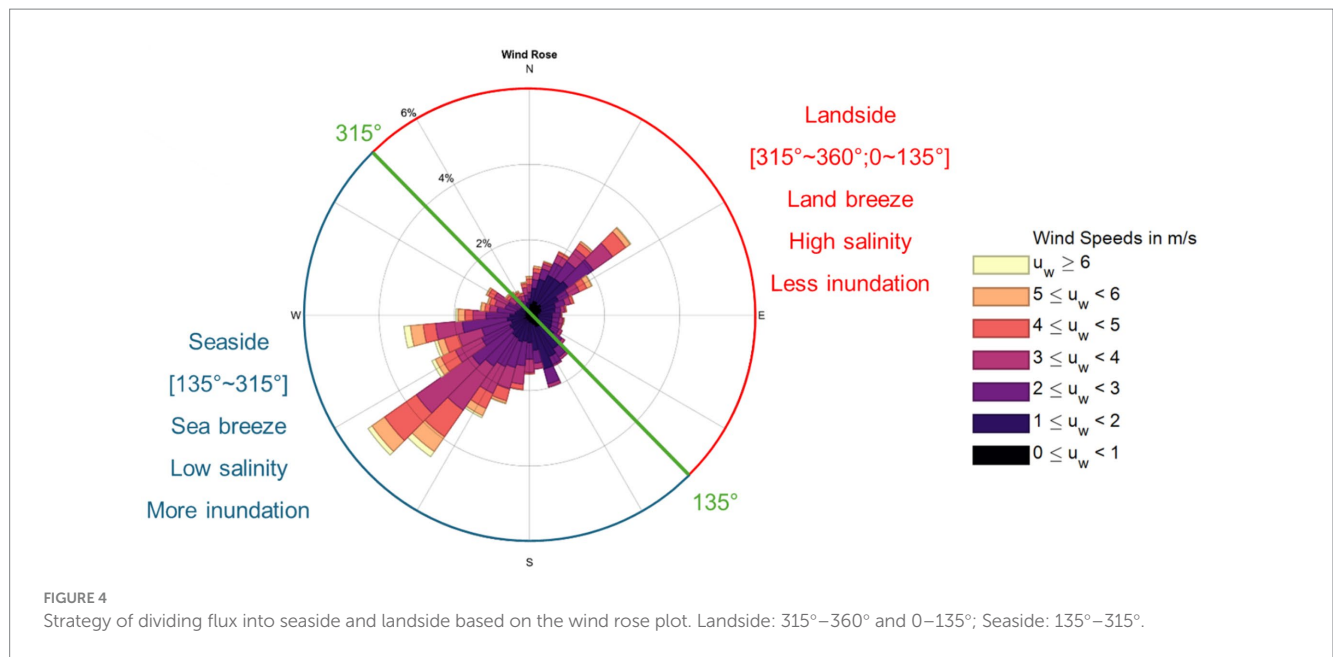
FIGURE 3 Workflow diagram for (a) data collection; (b) key indexes; and (c) statistical analysis.

and the sonic anemometer. Data collection lasted from November 8, 2017 to December 8, 2019. The sensors and field settings are summarized in [Supplementary Table S1](#).

The flux data was processed using EddyPro software (v 6.2.0, LI-COR, Lincoln, NE, United States) ([Abiodun, 2019](#)), including spike removal ([Mauder et al., 2013](#)), time lag corrections, coordinate rotation ([Wilczak et al., 2001](#)), and Webb-Pearman-Leuning density corrections ([Webb et al., 1980](#)). Gaps in the output data due to quality control and equipment malfunctions were filled using the REddyProc online processing tool using look-up table (LUT) and mean diurnal course (MDC) methods

([Wutzler et al., 2018](#)).¹ Due to the principle of EC measurements, the sensor fails to detect carbon flux from the landside when the wind blows from the seaside. This typically occurs between 11 a.m. and 4 p.m. local standard time when the NEP is large. In contrast, landside flux is usually detected at night and in the early morning when NEP is small. As a result, daytime landside carbon flux is missing from the measurement, making

¹ <https://www.bgc-jena.mpg.de/REddyProc/ui/REddyProc.php>



comparisons between seaside and landside flux unfair. Therefore, we use the averaged NEP value for each hour, month, and side (seaside and landside) to fill the missing data when the wind is from the opposite direction, ensuring that the impact of salinity on flux is not overestimated. For example, if there is a missing value at 13:00 on 01/01/2019 from the landside, we calculate the average NEP for all 13:00 readings from the landside throughout January to fill the missing value.

Ecosystem gross primary production (GPP) flux was partitioned from NEE and respiration (Reco) flux ($GPP = Reco - NEE$) using the REddyProc tool. Reco was estimated by the nighttime partitioning method (Reichstein et al., 2005). In this study, we reported net ecosystem production (NEP, defined as $NEP = -NEE$) instead of NEE for the net carbon uptake of the mangrove ecosystem. All variables were aggregated from hourly to daily scale, and data for days with more than 30% missing hourly values were excluded.

After gap filling, the flux footprint figure (Figure 2c) was generated using the Flux Footprint Prediction (FFP) online tool (Kljun et al., 2015),² based on the crosswind distribution of the flux footprint and the backward Lagrangian stochastic particle dispersion model (LPDM-B) used in the footprint parameterization. About 90% of the flux originated from a circle of 200 m radius around the tower (Figure 2c).

2.2.2 Other data

The tide level data was obtained from Flinders Ports Pty Ltd. It was measured using an air bubbler (Model 2100P, ES&S, Australia) at Port Adelaide (Outer Harbor), approximately 7 km west of the mangrove site (Flinders Ports Pty Ltd, 2024). To represent elevation, the 5-meter Australian Digital Elevation Model (DEM) derived from a LiDAR model was obtained from

Google Earth Engine (Geoscience Australia, 2015). Sentinel-2 (Copernicus Sentinel Data, 2024) band-11 and band-4 data from 2018 to 2019 from Google Earth Engine were used to calculate salinity stress (see section 2.3.2). Minutely solar radiation data (R_g , $W m^2$) was obtained from the Bureau of Meteorology recorded at the Adelaide airport (Australian Government, 2024).

2.3 Methods

2.3.1 Comparison strategy between seaside and landside sections

The eddy covariance station measured carbon flux from varying source areas depending on wind direction and speed. This situation provides an opportunity to compare the NEP of different source areas of the mangrove ecosystem.

To account for salinity differences, sea/land breezes, and tidal flooding effects, the carbon flux data were separated into two source sections using a line drawn at 135° and 315° on either side of the station (Figure 4). Mangroves on the landside (315° ~ 360° and 0 ~ 135°) are expected to experience higher salinity stress and less frequent tidal inundation than those on the seaside (135° ~ 315°). This situation makes it possible to investigate the salinity and tidal flooding effect on mangrove carbon flux. Meanwhile, the carbon flux from the landside source section tends to be under drier air from land breezes, and those from the seaside source section tend to be under moister air from sea breezes. Thus, the effects of sea/land breezes on mangrove carbon flux can be considered as well.

2.3.2 Salinity stress

Following Stong (2008), the salinity stress index (SSI) was calculated using Sentinel-2 band-11 (covering the wavelength range of 1,564–1,655 nm) and band-4 (covering the wavelength range of 650–680 nm) collected from 2018 to 2019, showing in Equation (1). The wavelengths for SSI are 1,680, 1,460, and 660 nm, which

² <https://geography.swansea.ac.uk/nkljun/ffp/www/>

correspond to band 11 and band 4 of the Sentinel-2 satellite. These wavelengths are highly sensitive to plant biochemical responses to soil salinity (Stong, 2008).

$$SSI = \frac{2\rho_{11}}{\rho_4} \quad (1)$$

where ρ is the reflectance of the corresponding band (subscript number) in Sentinel-2, with central wavelengths of 1,610 nm and 665 nm for band-11 and band-4, respectively. To illustrate the salinity gradient from each direction, SSI was averaged over five-degree intervals on the 90% flux footprint circle. It was then normalized to a range of 0–1 by its maximum and minimum values. The distribution of SSI can be found in section 3.3.

2.3.3 Sea/land breeze effects

To consider the impact of sea/land breezes, we proposed a dimensionless sea breeze index (W_b) using a trigonometric function based on wind direction, shown in Equation (2). The W_b was calculated as follows:

$$W_b = \sin\left(W_r - \frac{3\pi}{4}\right) \quad (2)$$

where W_r (radian) is the wind direction ($0 - 2\pi$). W_b ranges from -1 to 1 with $W_b = 0$ on the dividing line (straight from 135° to 315° , Figure 4). The distribution of W_b can be found in section 3.4.

2.3.4 Tidal flooding influence

Flooded fraction (F), or hydroperiod, is approximated as a linear function of relative elevation (Z) normalized between mean high water (MHW) and mean low water (MLW) following Jafari et al. (2024) and Morris et al. (2002), shown in Equation (3).

$$F = \frac{MHW - Z}{MHW - MLW} \quad (3)$$

where MHW and MLW are the arithmetic means of the high and low water heights observed each tidal day over the study period (Liu et al., 2014). F represents the fraction of time when a location is inundated, ranging from 0 (never flooded) to 1 (always flooded).

In this study, W_b and F are aggregated from hourly to daily scale during daytime (when $R_g > 10 \text{ W m}^{-2}$) for analysing the response of daily daytime carbon flux to salinity, wind, and tidal flooding conditions.

2.3.5 Temperature stress

Optimal temperature (T_{opt}) was defined as the threshold where the slope of NEP- T_a (GPP- T_a) curve changes sign from positive to negative (Alvarado-Barrientos et al., 2021). Due to the possible non-monotonic relationship between T_a on carbon sequestration, the data are divided into low- and high-temperature groups based on the T_{opt} . The purpose is to characterize the response of carbon sequestration to environmental variables (R_g , VPD, W_b , and SSI) under different T_a conditions.

2.3.6 Statistical analysis

One-way ANOVA tests (Dunn and Clark, 1986) were conducted to detect the differences in flux between the landside and seaside.

Pearson's correlations were then utilized to assess the relationships between carbon flux and environmental variables (R_g , T_a , VPD, W_b , SSI, and F). T_{opt} of carbon flux was identified using piecewise linear regressions with the lowest residual error (Okazak, 2024).

Path analysis (Land, 1969) was employed to quantify the response of carbon flux to meteorological and salinity factors for low- and high-temperature groups. The standardized path coefficient (β) in the path diagram was used to compare the direct and indirect effects of one variable on another (Finney, 1972; Hu and Lei, 2021). Path analysis models were constructed based on presumed causal relationships between flux and environmental drivers using the structural equation model (SEM) program in R Studio (Gana and Broc, 2019). These models were adjusted according to the modification indexes (MI) to show the change of model fit when a particular path was added or removed (Whittaker, 2012). The models were evaluated using the goodness-of-fit indexes, including comparative fit index (CFI) and standardized root mean square residual (SRMR). CFI characterizes the model's goodness of fit compared to an alternative model in reproducing the observed covariance matrix (Chen, 2007). SRMR represents the average standardized residuals between the observed and model-implied covariance matrices (Chen, 2007). Models meeting the criteria of $CFI \approx 1$ and $SRMR < 0.08$ were considered acceptable (Hopper et al., 2008; Schreiber et al., 2010). The analyses were restricted to daytime periods ($R_g > 10 \text{ W m}^{-2}$) to ensure that the fluxes were physiologically meaningful (Hu and Lei, 2021).

We hypothesize that R_g , T_a , VPD, SSI, and F have direct impacts on carbon flux, while W_b and R_g have indirect impacts by changing both T_a and VPD. T_a also indirectly affects carbon flux through VPD. Meanwhile, F has an indirect effect through SSI.

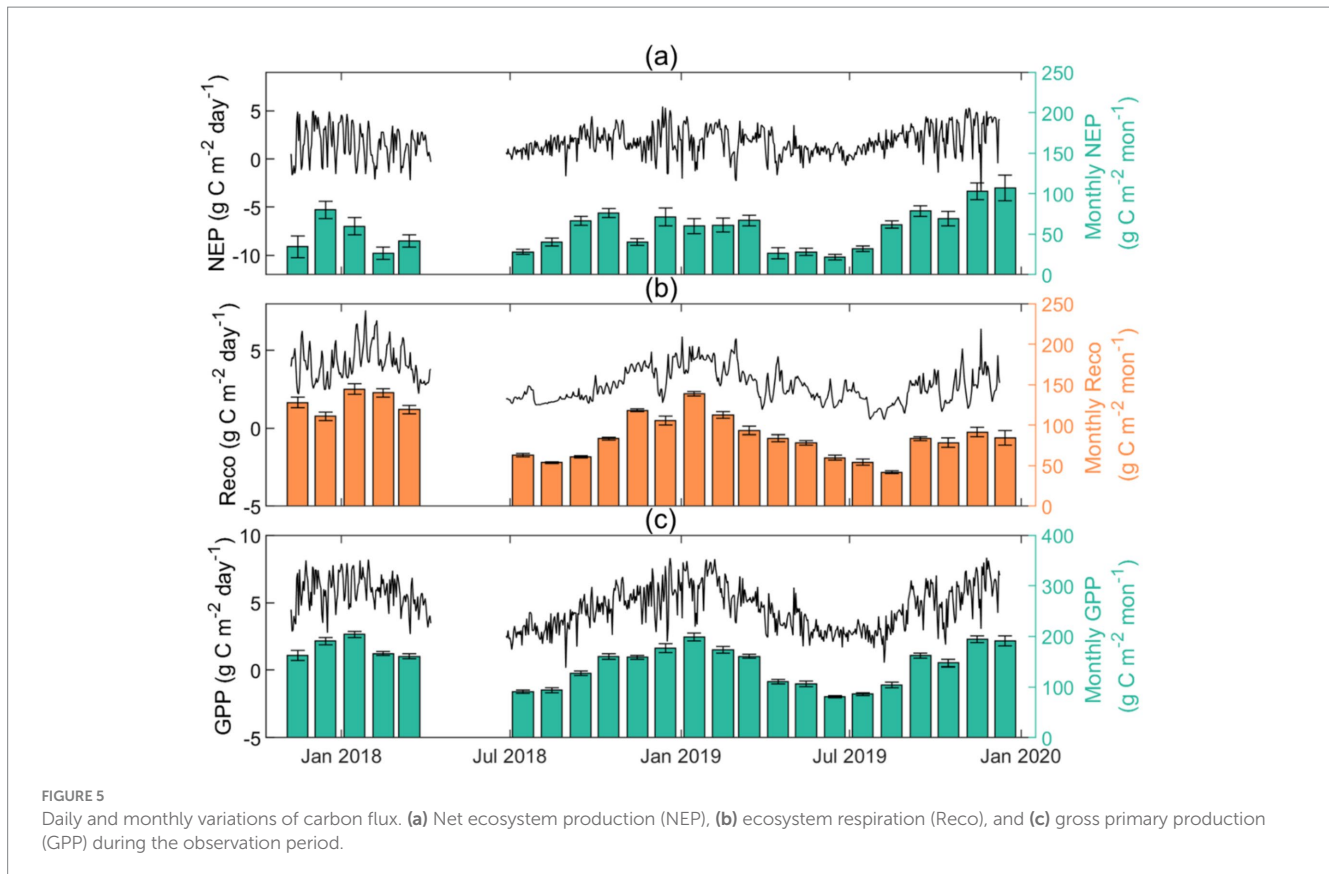
3 Results

3.1 Carbon sequestration rates

The diurnal, daily, and monthly NEP, Reco, and GPP exhibit evident seasonal cycles throughout the study period (Figure 5; Supplementary Figure S1). Daily NEP, Reco, and GPP are -3.3 to 5.0 , 0.6 to 7.6 , and 0.2 to $8.3 \text{ g C m}^{-2} \text{ day}^{-1}$, respectively (Figure 5). The highest monthly NEP ($107.4 \pm 15.8 \text{ g C m}^{-2} \text{ mon}^{-1}$), Reco ($144.4 \pm 6.6 \text{ g C m}^{-2} \text{ mon}^{-1}$), and GPP ($204.3 \pm 6.1 \text{ g C m}^{-2} \text{ mon}^{-1}$) occur in December or January (summer in the southern hemisphere), indicating higher carbon assimilation rates in summer (December, January, and February) and lower rates in winter (June, July, and August). Furthermore, the annual mean NEP, $645.8 \text{ g C m}^{-2} \text{ yr}^{-1}$, is close to the global mean of intertidal forested wetlands ($\sim 650 \text{ g C m}^{-2} \text{ yr}^{-1}$) (Lu et al., 2017). The annual mean Reco and GPP are 1106.7 and $1752.5 \text{ g C m}^{-2} \text{ yr}^{-1}$, respectively.

3.2 Directional differences in carbon flux

Daily NEP and GPP are consistently significantly higher on the seaside than on the landside ($p < 0.01$, Figures 6a,c). For NEP, peak values were approximately $5.5 \text{ g C m}^{-2} \text{ day}^{-1}$ on the seaside and $4.7 \text{ g C m}^{-2} \text{ day}^{-1}$ on the landside. A peak GPP of $9.2 \text{ g C m}^{-2} \text{ day}^{-1}$ on the seaside and of $7.0 \text{ g C m}^{-2} \text{ day}^{-1}$ on the landside indicate higher CO_2 assimilation by the seaside mangroves. In contrast, the difference in



daily Reco between the two sections is not significant ($p > 0.01$, Figure 6b). These differences in NEP and GPP between the two sections are arguably attributed to the effects of salinity and sea/land breezes.

3.3 Salinity stress index

The SSI map was divided into landside and seaside by the 135° – 315° line through the station (white dashed line in Figure 7a). The SSI in Figure 6b shows that mangroves on the landside experiences significantly higher salinity stress than those on the seaside. Figure 7b shows significant difference in SSI between the two regions ($p < 0.05$).

3.4 Sea/land breeze index (W_b)

Figure 8 shows the distribution of W_b , with $W_b = 0$ on the dividing line (green line from 135° to 315°) and reaching its extremes perpendicular to it (-1 at 45° and 1 at 225°). W_b increases toward the southwest and decreases toward the northeast from the division line. A positive (negative) W_b indicates winds from the seaside (landside) (Figure 8).

3.5 Flooded fraction (F)

Figure 9 shows the comparison of flooded fraction (F) between the landside and seaside. The seaside is subject to more frequent tidal inundations compared to those on the landside. Statistical analysis

confirms significant difference in F between the two sections ($p < 0.05$), suggesting hydrological variation likely influences ecosystem carbon exchange across the site.

3.6 The responses of carbon flux to air temperature, salinity and tidal flooding

Nonlinear $NEP-T_a$ and $GPP-T_a$ response curves, negative $NEP-SSI$ and $GPP-SSI$, and positive $NEP-F$ and $GPP-F$ relationships are obtained based on the correlation matrix (Supplementary Figure S2). As shown in Figures 10a,b, T_{opt} determined by piecewise linear regression equation is $20.4^{\circ}C$ for NEP. NEP increases with T_a until T_{opt} , above which NEP drops sharply. Although the $GPP-T_a$ relationship also exhibits nonlinear behavior, with GPP increasing with T_a and continuing to rise at a reduced rate beyond the $21.3^{\circ}C$ breakpoint. However, this breakpoint does not align with the definition of an optimal temperature in this study, which requires a shift from positive to negative slope. The slight increase in GPP is likely driven by rising Reco rates at higher temperatures. Therefore, Figures 10b,c suggests no clear T_{opt} for GPP and Reco in this study.

The negative relationships of SSI with NEP and GPP persist through most of the seasons (Figures 10d,e), with more pronounced negative effects of SSI on NEP and GPP during summer (green dots in Figures 10d,e), suggesting that salinity stress limited landside mangrove carbon uptake. For the tidal flooding influence, the positive relationship of F with NEP and GPP are stronger in the summer (green dots in Figure 10g,h), indicating that tidal inundation likely enhanced carbon sequestration in the seaside mangrove ecosystem but reduced it in the landside. Reco shows no significant response to SSI or F (Figures 10f,i).

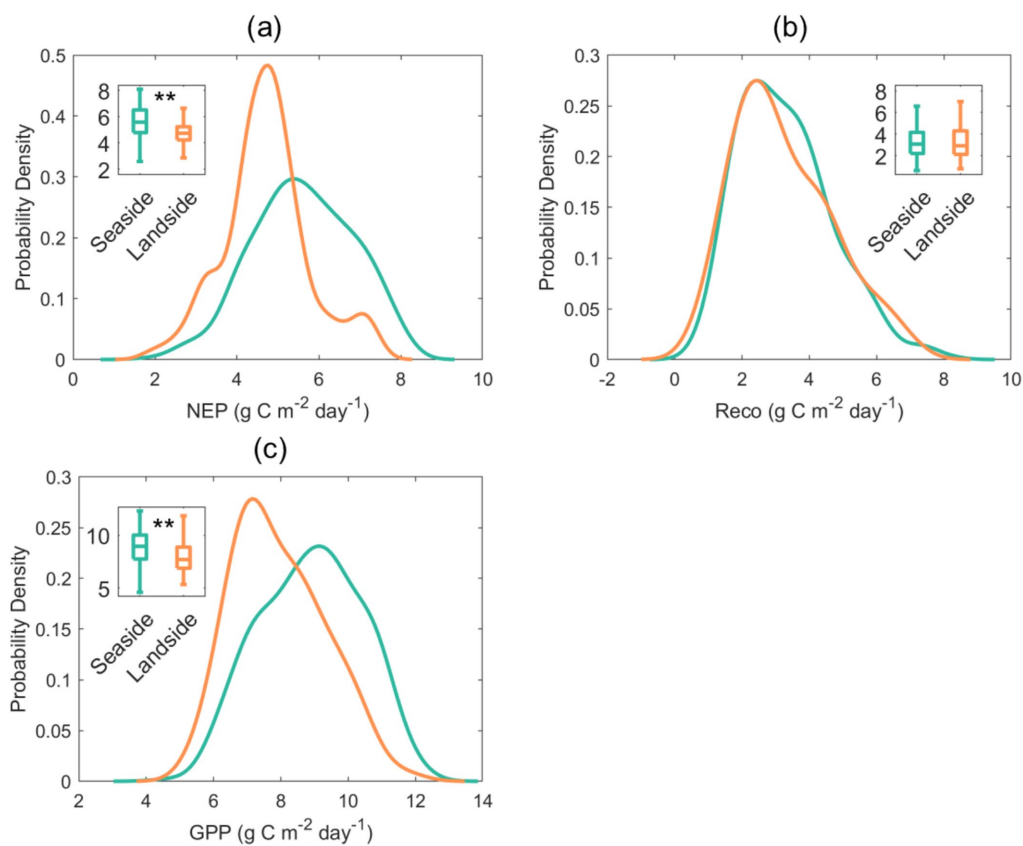


FIGURE 6 Probability density distribution of daily daytime. **(a)** Net ecosystem production (NEP), **(b)** ecosystem respiration (Reco), and **(c)** gross primary production (GPP) from seaside (green) and landside (orange). In boxplots indicate significant differences in CO₂ flux from two sides according to one way ANOVA tests at 1% level.

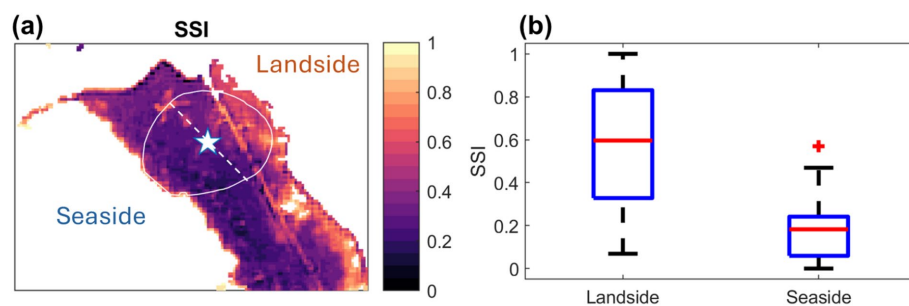


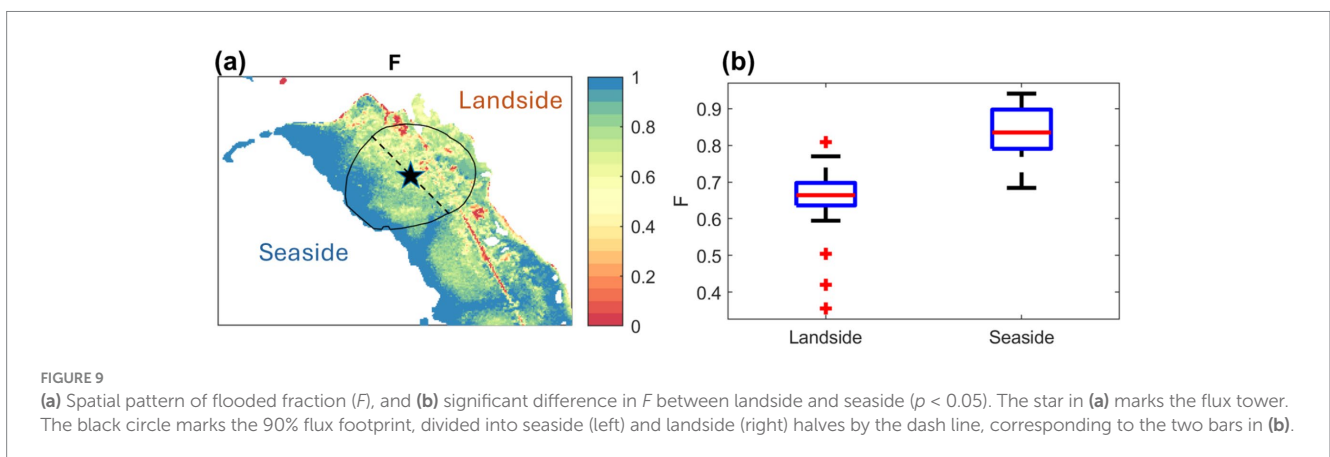
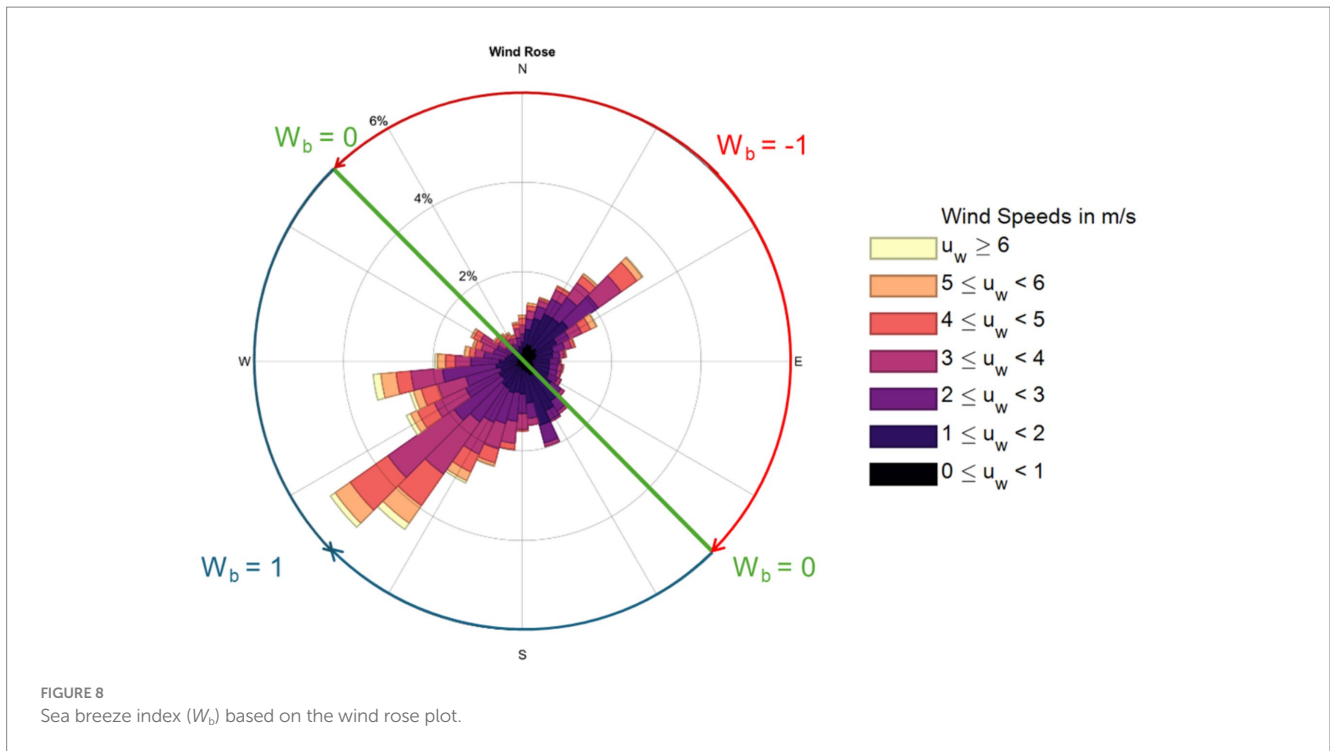
FIGURE 7 **(a)** Spatial pattern of salinity stress index (SSI), and **(b)** significant difference in SSI between landside and seaside ($p < 0.05$). The star in **(a)** marks the flux tower. The white circle shows the 90% flux footprint, divided into seaside (left) and landside (right) halves by the dash line, corresponding to the two bars in **(b)**.

3.7 Environmental controls on NEP

Path diagrams in Figure 11 show the direct and indirect effects of each environmental variable on daily daytime NEP at low- and high-temperature. The total effects are calculated in Supplementary Table S2.

At low temperatures, NEP is directly enhanced by R_g (Figure 11a), with strengths of 0.33 ($\beta = 0.33$), and indirectly enhanced by F ($\beta = 0.15$), but directly decreased by SSI ($\beta = -0.21$). Meanwhile, T_a ,

VPD, and W_b impacts are not significant for NEP at low temperatures (Figure 11a). Under high temperatures (Figure 11b), NEP is reduced by high T_a , high VPD, and SSI, but enhanced by W_b and F . T_a is the dominant negative regulator of NEP with a total effect of -0.59 , including an indirect effect through VPD. W_b alleviates the stress of high T_a and VPD on NEP with a strength of 0.23. Additionally, F mitigates the salinity stress on NEP with a strength of 0.14 (Supplementary Table S2).



In summary, R_g and SSI are the dominant positive and negative drivers at low temperature, increasing NEP by 48% and decreasing it by 30%, respectively. F increases NEP by 20%. Conversely, W_b and T_a are the dominant positive and negative drivers at high temperature, increasing NEP by 16% and decreasing it by 40%, respectively. SSI decreases NEP by 13%, and F increases NEP by 10%.

4 Discussion

4.1 Effects of salinity gradient and tidal inundation on NEP

Higher salinity occurs on the landside at the study site due to the adjacent salt evaporation ponds and the absence of freshwater runoff into the ecosystem. This situation is very different from the other studies, where higher salinity is typically on the seaside given

freshwater discharges to the sea through the ecosystem (Ahmed et al., 2022; Gou et al., 2023; Heinsch, 2004). Due to local land use involving salt evaporation ponds, a reverse salinity gradient occurred (Figure 2). The ponds could potentially be one reason for the serious dieback event in 2020 (Water, 2021).

Our analysis shows that salinity stress can be mitigated by tidal inundation at the site scale (Figure 11), but likely due to frequent inundation on the seaside. As shown in Figure 12, NEP tends to be higher when tidal flooding is more frequent ($F > 0.7$), and salinity stress is low ($SSI < 0.3$). The landside experiences both higher salinity stress and lower tidal inundation, resulting in a combined negative impact on carbon assimilation in landside mangroves. Tidal flooding may mitigate salinity stress in landside mangroves by flushing salt out, but is limited by the higher elevation (Figure 9). Therefore, the differential extent of tidal inundation amplifies salinity contrast between seaside and landside areas, thereby influencing the corresponding carbon uptake rates.

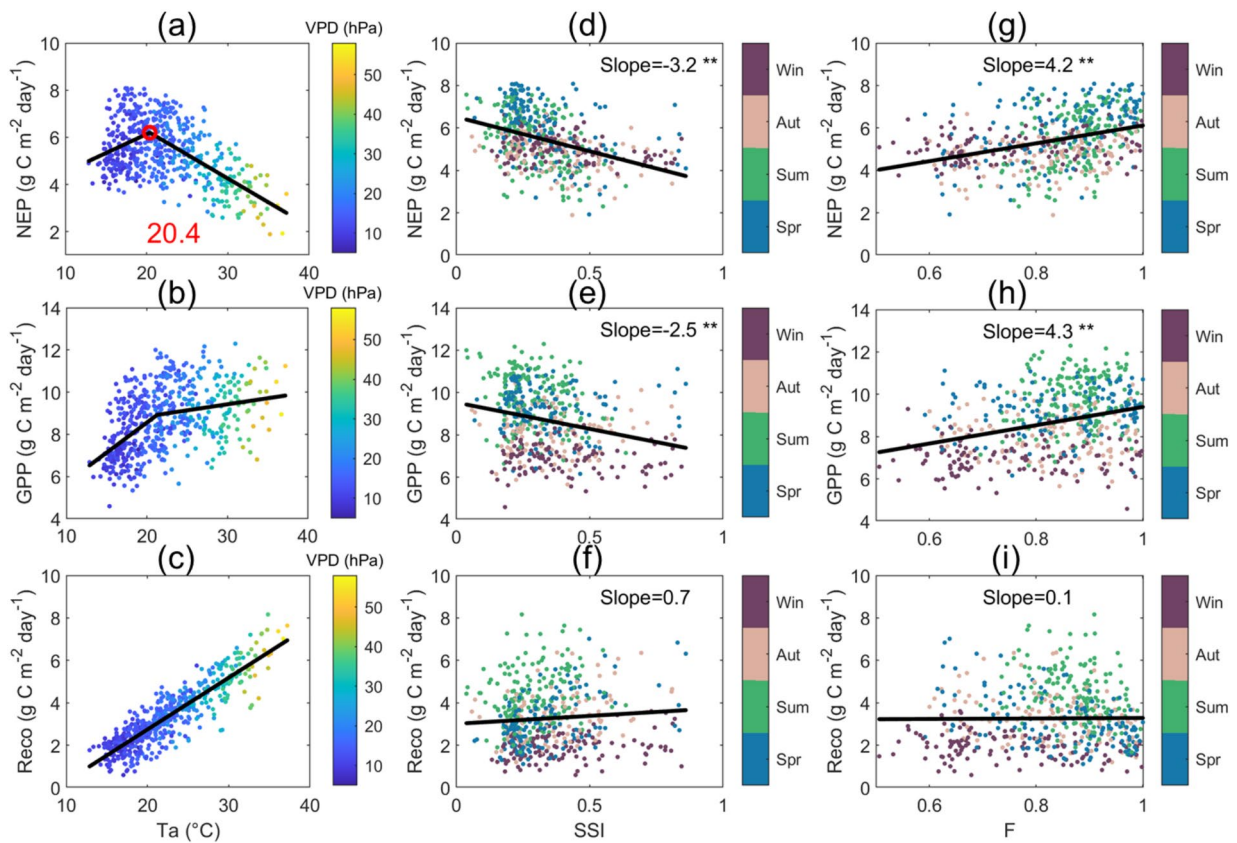


FIGURE 10
 Dependence of daily daytime (a) NEP, (b) GPP, and (c) Reco on daytime T_a along the VPD gradient, and relationships of daytime (d,g) NEP, (e,h) GPP, and (f,i) Reco with SSI and F . SSI and F were averaged for five-degree intervals on the 90% flux footprint. Black lines in (a,b) represent piecewise linear regressions with two connected segments. Red circles and numbers in (a) indicate the optimal temperature (T_{opt} , °C) for NEP. Black solid lines in (c–i) show linear regressions for all observed data.

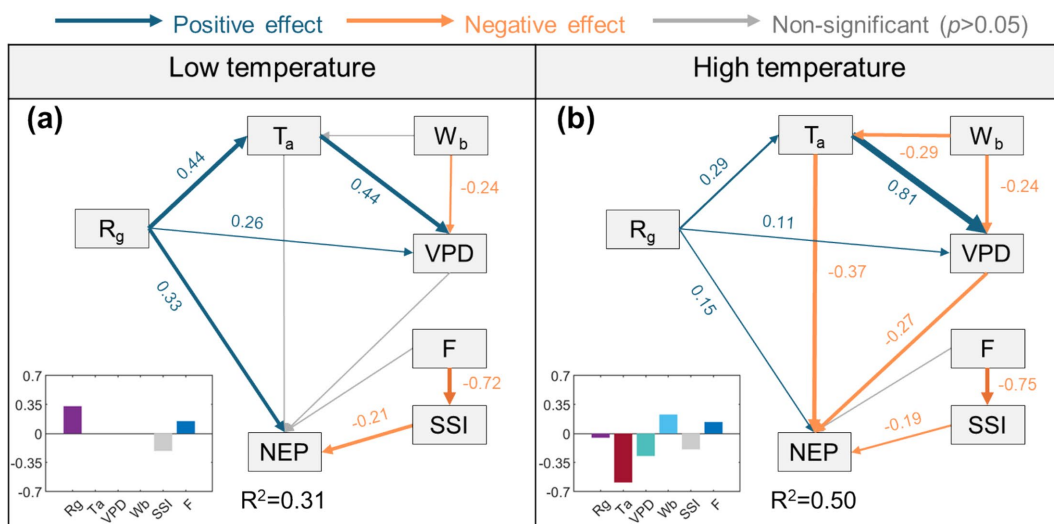
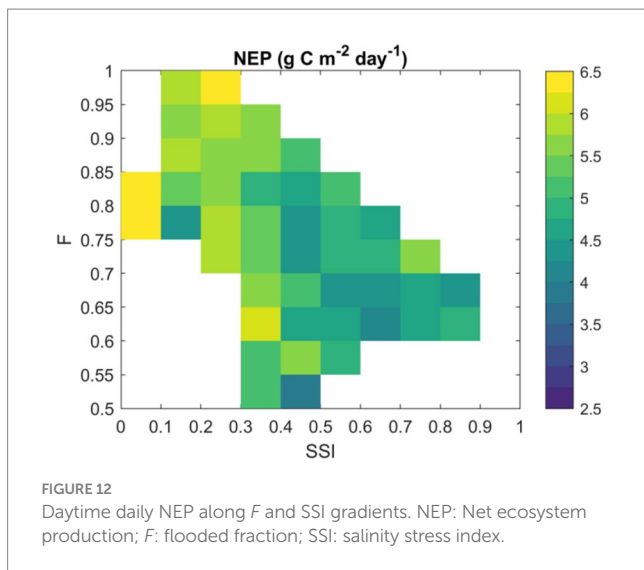


FIGURE 11
 Path diagrams for effects of environmental variables (R_g , T_a , VPD, W_b , SSI, and F) on daytime daily net ecosystem production (NEP, g C m⁻² day⁻¹) with low-temperature (a) and high-temperature (b) separated by the optimal temperature (T_{opt}). Significant ($p \leq 0.01$) positive and negative paths were represented by blue and orange arrows, along with the standardized path coefficients (β); no path coefficient was given for the non-significant path (gray arrows, $p > 0.01$). The bar chart in each subplot represents the total effect of each driver. R^2 : Coefficient of determination. R_g : Shortwave solar radiation (W m⁻²); T_a : Air temperature (°C); VPD: Vapor pressure deficit (hPa); W_b : Sea breeze index; SSI: Salinity stress index; F : Flooded fraction.



Some research shows that sea level rise tends to reduce carbon uptake in subtropical coastal marshes by limiting root-zone oxygen, restricting CO₂ diffusion, and increasing ionic and osmotic stress in plants and soil (Li et al., 2020; Pezeshki, 2001). The response of deltaic mangrove ecosystems to sea level rise depends on the vertical accretion of seaward expansion keeping pace with the rising sea level (Dai et al., 2024; Lovelock et al., 2015; Xiong et al., 2024). In contrast to subtropical or deltaic areas, our site exhibits a different response. More frequent tidal inundation sea level rise resulting from enhance may NEP by reducing salinity stress on landside mangroves.

4.2 Effects of temperature stress and sea breezes on NEP under global warming

High temperature decreases mangrove photosynthesis by reducing stomatal conductance (Krauss et al., 2008; Lovelock et al., 2016). An optimal temperature range for NEP ($T_{opt,r}$, 16–24 °C) is observed along the T_a gradient when SSI < 0.3 (Figure 13a). NEP declines beyond this range. The $T_{opt,r}$ at this study site is lower than that (22–30 °C) reported for leaf-level photosynthesis maximization (Duffy et al., 2021; Moore et al., 1973; Noor et al., 2015; Paramita Nandy et al., 2007; Reef et al., 2016), and lower than that (27 °C) of a tropical mangrove ecosystem reported in Alvarado-Barrientos et al. (2021); 29.8 °C of a subtropical riverine mangrove (Barr, 2005); and 26.8 °C of a semi-arid basin mangrove (Leopold et al., 2016). This difference can be explained by the fact that the mangrove species in this study is a temperate mangrove, growing under temperatures lower than those in subtropical or tropical areas.

Under high-temperature conditions, NEP is significantly enhanced by sea breezes, which act as a dominant positive driver (Figure 11). Sea breezes reduce air temperature and atmospheric moisture stress, alleviating heat and vapor pressure deficit constraints on stomatal conductance, thereby increasing carbon uptake. In contrast, sea breezes had no significant effect on NEP under low-temperature conditions (Figure 11), suggesting that its role is most critical during periods of heat stress. These findings align with Zhu et al. (2021) that regular afternoon sea breezes cool and moisten the atmosphere, indirectly promoting carbon assimilation in a

subtropical mangrove ecosystem. In this study area, significant sea breeze cooling mostly occurs on hot summer days, when sea breezes are most frequent (Masouleh, 2015), and their cooling effect is particularly important during heatwave conditions (Zhou et al., 2021; Guan et al., 2016). In contrast, during cooler seasons (early spring, late autumn, and winter), sea breezes are weaker and less developed. In this period, mangrove benefits from warmer temperatures. Thus, sea breezes have little effect on NEP. Our analysis highlights the important but often overlooked role of sea breezes in regulating mangrove carbon dynamics under climate warming scenarios.

Global warming causes shifts in temperature patterns, leading to more frequent and severe heatwaves (Perkins-Kirkpatrick and Lewis, 2020). According to long-term T_a records from the Adelaide airport, the frequency of T_a within the $T_{opt,r}$ (16–24 °C) increased from 36.9 to 41.2% (Figure 13b; Supplementary Table S4), and T_a above 24 °C (high T_a) increased from 7.9 to 10.2%, and T_a below 16 °C (low T_a) decreased from 55.4 to 48.6% during 1956–1980 and 2001–2023. Due to the cooling effect of sea breezes (Papanastasiou et al., 2010; Zhou et al., 2021), extreme high T_a increased slightly (2.3%) compared to the optimal temperature range (4.3%, Supplementary Table S4). The decrease in NEP due to high T_a for temperate mangroves could be offset by the increase in NEP within $T_{opt,r}$ (Supplementary Table S4), assuming other conditions remain unchanged, resulting in a net increase of 0.034 g C m⁻² day⁻¹ (12.4 g C m⁻² yr⁻¹) in NEP (Supplementary Table S4).

Global warming is generally expected to decrease terrestrial carbon sequestration (Duffy et al., 2021). Zhu et al. (2021) pointed out that mangrove wetlands could become a weaker blue carbon sink in response to global warming and sea level rise due to the strong negative impacts of rising air temperature and tidal inundation. However, our analysis suggests that NEP could increase in the future for the studied temperate mangrove forest as sea level rise may lead to more extended tidal inundation to alleviate salinity stress, and warming can lead to more frequent optimal temperature days for carbon uptake. The difference between this study and Zhu et al. (2021) may be attributed to different climatic and environmental conditions: Zhu et al.'s study was conducted in a subtropical region, while our study site is in a temperate climate zone. Moreover, our site lacks freshwater input, and the salinity gradient is strongly influenced by human activities (salt ponds). These local conditions may shape the main environmental factors affecting carbon dynamics, which could explain why ecosystems respond differently to warming and sea level rise.

4.3 Uncertainties

This study has limitations. Separating the NEE data into the landside and seaside sources leads to gaps in each time series. The missing half-an-hourly data points were replaced by the corresponding averages of available data in the same month across years. Jammet et al. (2017) tested artificial neural network (ANN) models to gap-fill methane (CH₄) emissions and CO₂ exchange from a fen and a lake at the hourly scale, but found this approach unreliable for lake CO₂ exchange. They therefore used mean values for seasonal comparisons to avoid large uncertainties. We followed a similar approach, as our dataset covers only 2 years, and more advanced

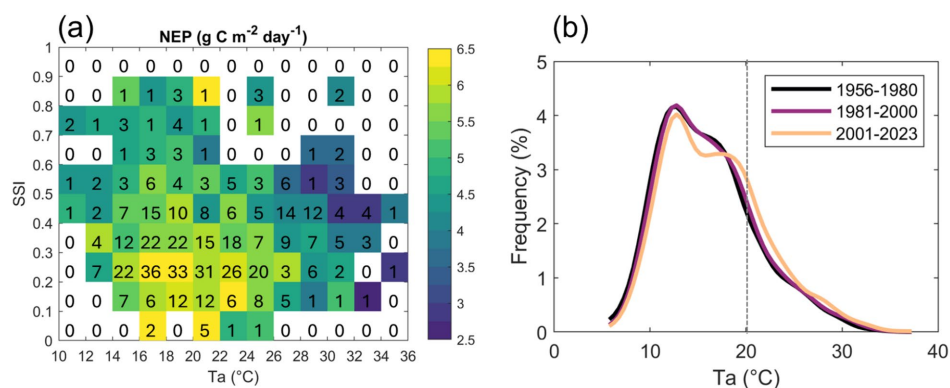


FIGURE 13
Daytime daily NEP along (a) T_a and SSI gradients, and (b) frequency of T_a in different periods. Numbers in (a) represent the count of data points used to calculate the mean value in each grid. Gray dotted line in (b) indicates the optimal temperature (T_{opt}). NEP: net ecosystem production; T_a : air temperature; SSI: salinity stress index.

methods such as machine learning often require large sample sizes and may introduce additional uncertainty. At the study site, 10-fold cross-validation ($k = 10$) showed that the average root mean square error (RMSE) for the two sides was $2.63 \mu\text{mol m}^{-2} \text{s}^{-1}$ (5.89% of the half-hourly NEE range) with $R^2 = 0.76$, and about 35% of the gaps were filled.

The study partitioned Reco from NEP based on the Reco-temperature relationship derived from nighttime measurement. However, inundation may also affect Reco, which is not considered in the partitioning method. Nonetheless, these sources of uncertainty do not affect the main results as the focus of this study is on net CO_2 exchange rather than GPP.

Another limitation is that lateral advection was not explicitly accounted for. The EC measurements are most accurate over extended homogeneous surfaces under steady environmental conditions (Baldocchi, 2003). Yet such ideal conditions do not exist in practice. Characterizing advection in heterogeneous environments remains challenging in micrometeorology (Levy et al., 2020). Given the contrast between the landside and seaside within the footprint of the EC measurements has the length scale (~ kilometers) is much greater than the length scale of vertical gradients of gas concentrations (~ 10 meters), the effect of lateral advection on the observed fluxes was arguably negligible hence not considered in this study.

5 Conclusions

In this study, we investigated the responses of carbon flux to salinity, air temperature, sea/land breezes, and tidal water table in a temperate mangrove forest in South Australia using an eddy covariance system.

Significant differences in carbon flux along a transect of over 300 m were revealed between the seaside and landside sections of the mangrove forest. The negative effects of salinity on carbon flux persist through most of the seasons. The positive relationship between F and NEP suggests tidal inundation enhancing carbon sequestration in the seaside mangrove ecosystem. An optimal daily temperature range of 16–24 °C was found with the peak at 20.4 °C for NEP. At low temperatures, R_g and SSI were dominant

positive and negative drivers of NEP, increasing NEP by 48% and decreasing it by 30%, respectively. F increases NEP by 20%. At high temperatures, T_a was the dominant negative drivers for NEP, decreasing it by 40%. Sea breeze cooling was a positive dominant driver by reducing the high T_a and VPD stress on NEP, increasing NEP by 16%. SSI decreases NEP by 13%, and F increases NEP by 10%. In addition, NEP at this particular site was enhanced by an increasing frequency in the optimal temperature range, but reduced by more frequent high T_a , resulting in a net increase of $12.4 \text{ g C m}^{-2} \text{ yr}^{-1}$ in NEP from 1956–1980 to 2001–2023.

These results provide a baseline for predicting the response of temperate mangroves to future warming and sea level rise. The carbon flux data obtained in this study provide a reference for analysing the impacts of global and local environmental changes on temperate mangrove ecosystems, and support the effective management of mangrove forests under temperature and salinity stress.

Data availability statement

The raw data supporting the conclusions of this article will be made available by the authors, without undue reservation.

Author contributions

WY: Writing – review & editing, Investigation, Software, Conceptualization, Writing – original draft, Visualization, Validation, Resources, Formal analysis, Methodology. HG: Conceptualization, Investigation, Data curation, Supervision, Methodology, Writing – review & editing, Resources, Funding acquisition, Formal analysis, Project administration. JW: Writing – review & editing, Supervision, Formal analysis, Investigation, Methodology, Resources. OA: Writing – review & editing, Formal analysis, Data curation, Investigation. YZ: Formal analysis, Data curation, Writing – review & editing, Investigation. OB: Funding acquisition, Resources, Writing – review & editing, Project administration, Formal analysis, Data curation, Investigation, Supervision.

Funding

The author(s) declared that financial support was received for this work and/or its publication. WY and YZ were partly supported by China Scholarship Council. JW's research is supported by US NSF grant NNA2126797.

Acknowledgments

Sabine Dittmann and Luke Mosley assisted site selection. Lawrence Burk, Na Liu, Lihui Tian, and Xanthia Gleeson assisted field installation and data collection. City of Salisbury provided access to the field site. Zhechen Zhang contributed to some discussion of the result. We acknowledge Flinders Ports Pty Ltd. for providing the tide data.

Conflict of interest

The author(s) declared that this work was conducted in the absence of any commercial or financial relationships that could be construed as a potential conflict of interest.

References

- Abiodun, O. (2019). The evaluation and improvement of the maximum entropy production (MEP) evapotranspiration method at graduated spatial scales-point, catchment and continental scales: Flinders University, College of Science and Engineering. Adelaide.
- Ahmed, S., Sarker, S. K., Friess, D. A., Kamruzzaman, M., Jacobs, M., Islam, M. A., et al. (2022). Salinity reduces site quality and mangrove forest functions. From monitoring to understanding. *Sci. Total Environ.* 853:158662. doi: 10.1016/j.scitotenv.2022.158662
- Alvarado-Barrientos, M. S., López-Adame, H., Lazcano-Hernández, H. E., Arellano-Verdejo, J., and Hernández-Arana, H. A. (2021). Ecosystem-atmosphere exchange of CO₂, water, and energy in a basin mangrove of the northeastern coast of the Yucatan peninsula. *J. Geophys. Res. Biogeosci.* 126:e2020JG005811. doi: 10.1029/2020jg005811
- Australian Government (2024). One Minute Solar Data produced with the support of the through the Australian Solar Institute. Available online at: <https://reg.bom.gov.au/climate/data/oneminsolar/about-IDCJAC0022.shtml> (accessed [01 06, 2026]).
- Baldocchi, D. D. (2003). Assessing the eddy covariance technique for evaluating carbon dioxide exchange rates of ecosystems: past, present and future. *Glob. Change Biol.* 9, 479–492. doi: 10.1046/j.1365-2486.2003.00629.x
- Barr, J. G. (2005). Carbon assimilation by riverine mangroves in the Florida Everglades: University of Virginia. Charlottesville.
- Cahyaningsih, A. P., Deanova, A. K., Pristiawati, C. M., Ulumuddin, Y. I., Kusumaningrum, L., and Setyawan, A. D. (2022). Causes and impacts of anthropogenic activities on mangrove deforestation and degradation in Indonesia. *Int. J. Bonorowo Wetlands* 12, 12–22. doi: 10.13057/bonorowo/w120102
- Castañeda-Moya, E., Rivera-Monroy, V. H., and Twilley, R. R. (2006). Mangrove zonation in the dry life zone of the Gulf of Fonseca, Honduras. *Estuar. Coasts* 29, 751–764. doi: 10.1007/BF02786526
- Chen, F. F. (2007). Sensitivity of goodness of fit indexes to lack of measurement invariance. *Struct. Equ. Model. Multidiscip. J.* 14, 464–504. doi: 10.1080/10705510701301834
- Chung, C. T. Y., Hope, P., Hutley, L. B., Brown, J., and Duke, N. C. (2023). Future climate change will increase risk to mangrove health in northern Australia. *Commun. Earth Environ.* 4:192. doi: 10.1038/s43247-023-00852-z
- Copernicus Sentinel Data (2024). Sentinel-7 image courtesy of the European Space Agency. Available online at: https://developers.google.com/earth-engine/datasets/catalog/COPERNICUS_S2_SR_HARMONIZED (accessed [01 06, 2026]).
- Dai, Z., Long, C., Mei, X., Fagherazzi, S., and Xiong, Y. (2024). Overestimation of mangroves deterioration from sea level rise in tropical deltas. *Geophys. Res. Lett.* 51:e2024GL109675. doi: 10.1029/2024gl109675
- Dittmann, S., Mosley, L., Stangoulis, J., Nguyen, V. L., Beaumont, K., Dang, T., et al. (2022). Effects of extreme salinity stress on a temperate mangrove ecosystem. *Front. For. Glob. Change* 5:859283. doi: 10.3389/ffgc.2022.859283
- Duffy, K. A., Schwalm, C. R., Arcus, V. L., Koch, G. W., Liang, L. L., and Schipper, L. A. (2021). How close are we to the temperature tipping point of the terrestrial biosphere? *Sci. Adv.* 7:eay1052. doi: 10.1126/sciadv.aay1052
- Duke, N., Ball, M., and Ellison, J. (1998). Factors influencing biodiversity and distributional gradients in mangroves. *Glob. Ecol. Biogeogr. Lett.* 7, 27–47. doi: 10.2307/2997695
- Duke, N. C., Kovacs, J. M., Griffiths, A. D., Preece, L., Hill, D. J. E., van Oosterzee, P., et al. (2017). Large-scale dieback of mangroves in Australia's Gulf of Carpentaria: a severe ecosystem response, coincidental with an unusually extreme weather event. *Mar. Freshw. Res.* 68, 1816–1829. doi: 10.1071/MF16322
- Dunn, O. J., and Clark, V. A. (1986). Applied statistics: Analysis of variance and regression. Hoboken. John Wiley & Sons, Inc.
- Farzanmanesh, R., Khoshelham, K., Volkova, L., Thomas, S., Ravelonjatovo, J., and Weston, C. J. (2024). Quantifying mangrove aboveground biomass changes: analysis of conservation impact in blue forests projects using sentinel-2 satellite imagery. *For. Ecol. Manag.* 561:121920. doi: 10.1016/j.foreco.2024.121920
- Finney, J. M. (1972). Indirect effects in path analysis. *Sociol. Methods Res.* 1, 175–186. doi: 10.1177/004912417200100202
- Flinders Ports Pty Ltd (2024). Tide Gauge Metadata and Observed Monthly Sea Levels and Statistics [Dataset]. Available online at: <http://www.bom.gov.au/oceanography/projects/ntc/monthly/index.shtml> (accessed [01 06, 2026]).
- Gana, K., and Broc, G. (2019). Structural equation modeling with lavaan: John Wiley & Sons. London.
- Geoscience Australia (2015). Digital elevation model (DEM) of Australia derived from LiDAR 5 metre grid [dataset]. doi: 10.4225/25/5652419862E23
- Gilman, E. L., Ellison, J., Duke, N. C., and Field, C. (2008). Threats to mangroves from climate change and adaptation options: a review. *Aquat. Bot.* 89, 237–250. doi: 10.1016/j.aquabot.2007.12.009
- Goldstein, G., and Santiago, L. S. (2016). Tropical tree physiology: Cham. Springer.
- Gou, R., Buchmann, N., Chi, J., Luo, Y., Mo, L., Shekhar, A., et al. (2023). Temporal variations of carbon and water fluxes in a subtropical mangrove forest: insights from a decade-long eddy covariance measurement. *Agric. For. Meteorol.* 343:109764. doi: 10.1016/j.agrformet.2023.109764
- Gu, X., Zhao, H., Peng, C., Guo, X., Lin, Q., Yang, Q., et al. (2022). The mangrove blue carbon sink potential: evidence from three net primary production assessment methods. *For. Ecol. Manag.* 504:119848. doi: 10.1016/j.foreco.2021.119848

Generative AI statement

The author(s) declared that Generative AI was not used in the creation of this manuscript.

Any alternative text (alt text) provided alongside figures in this article has been generated by Frontiers with the support of artificial intelligence and reasonable efforts have been made to ensure accuracy, including review by the authors wherever possible. If you identify any issues, please contact us.

Publisher's note

All claims expressed in this article are solely those of the authors and do not necessarily represent those of their affiliated organizations, or those of the publisher, the editors and the reviewers. Any product that may be evaluated in this article, or claim that may be made by its manufacturer, is not guaranteed or endorsed by the publisher.

Supplementary material

The Supplementary material for this article can be found online at: <https://www.frontiersin.org/articles/10.3389/fclim.2025.1720464/full#supplementary-material>

- Guan, H., Kumar, V., Clay, R., Kent, C., Bennett, J., Ewenz, C., et al. (2016). Temporal and spatial patterns of air temperature in a coastal city with a slope base setting. *J. Geophys. Res. Atmos.* 121, 5336–5355. doi: 10.1002/2016jd025139
- Heinsch, F. (2004). Carbon dioxide exchange in a high marsh on the Texas Gulf Coast: effects of freshwater availability. *Agric. For. Meteorol.* 125, 159–172. doi: 10.1016/j.agrformet.2004.02.007
- Hopper, D., Coughlan, J., and Mullen, M. R. (2008). Structural equation modeling: guidelines for determining model fit. *Electron. J. Bus. Res. Methods* 6, 53–60.
- Hu, X., and Lei, H. (2021). Fifteen-year variations of water use efficiency over a wheat-maize rotation cropland in the North China plain. *Agric. For. Meteorol.* 306:108430. doi: 10.1016/j.agrformet.2021.108430
- Jafari, N. H., Harris, B. D., Morris, J. T., and Cadigan, J. A. (2024). Interplay of hydroperiod on root shear strength for coastal wetlands. *Geophys. Res. Lett.* 51:e2023GL106531. doi: 10.1029/2023gl106531
- Jammet, M., Dengel, S., Kettner, E., Parmentier, F.-J. W., Wik, M., Crill, P., et al. (2017). Year-round CH₄ and CO₂ flux dynamics in two contrasting freshwater ecosystems of the subarctic. *Biogeosciences* 14, 5189–5216. doi: 10.5194/bg-14-5189-2017
- Jaramillo, F., Licero, L., Ahlen, I., Manzoni, S., Rodríguez-Rodríguez, J. A., Guittard, A., et al. (2018). Effects of hydroclimatic change and rehabilitation activities on salinity and mangroves in the Ciénaga Grande de Santa Marta, Colombia. *Wetlands* 38, 755–767. doi: 10.1007/s13157-018-1024-7
- Jia, M., Wang, Z., Mao, D., Ren, C., Song, K., Zhao, C., et al. (2023). Mapping global distribution of mangrove forests at 10-m resolution. *Sci. Bull. (Beijing)* 68, 1306–1316. doi: 10.1016/j.scib.2023.05.004
- Jimenez, J. A., Lugo, A. E., and Cintron, G. (1985). Tree mortality in mangrove forests. *Biotropica* 17, 177–185. doi: 10.2307/2388214
- Jones, M. O., Jones, L. A., Kimball, J. S., and McDonald, K. C. (2011). Satellite passive microwave remote sensing for monitoring global land surface phenology. *Remote Sens. Environ.* 115, 1102–1114. doi: 10.1016/j.rse.2010.12.015
- Kljun, N., Calanca, P., Rotach, M. W., and Schmid, H. P. (2015). A simple two-dimensional parameterisation for flux footprint prediction (FFP). *Geosci. Model Dev.* 8, 3695–3713. doi: 10.5194/gmd-8-3695-2015
- Krauss, K. W., Lovelock, C. E., McKee, K. L., López-Hoffman, L., Ewe, S. M. L., and Sousa, W. P. (2008). Environmental drivers in mangrove establishment and early development: a review. *Aquat. Bot.* 89, 105–127. doi: 10.1016/j.aquabot.2007.12.014
- Krauss, K. W., McKee, K. L., Lovelock, C. E., Cahoon, D. R., Saintilan, N., Reef, R., et al. (2014). How mangrove forests adjust to rising sea level. *New Phytol.* 202, 19–34. doi: 10.1111/nph.12605
- Land, K. C. (1969). Principles of path analysis. *Sociol. Methodol.* 1, 3–37. doi: 10.2307/270879
- Leopold, A., Marchand, C., Renchon, A., Deborde, J., Quiniou, T., and Allenbach, M. (2016). Net ecosystem CO₂ exchange in the “Coeur de Voh” mangrove, New Caledonia: effects of water stress on mangrove productivity in a semi-arid climate. *Agric. For. Meteorol.* 223, 217–232. doi: 10.1016/j.agrformet.2016.04.006
- Levy, P., Drewer, J., Jammet, M., Leeson, S., Friberg, T., Skiba, U., et al. (2020). Inference of spatial heterogeneity in surface fluxes from eddy covariance data: a case study from a subarctic mire ecosystem. *Agric. For. Meteorol.* 280:107783. doi: 10.1016/j.agrformet.2019.107783
- Li, Y. L., Guo, H. Q., Ge, Z. M., Wang, D. Q., Liu, W. L., Xie, L. N., et al. (2020). Sea-level rise will reduce net CO₂ uptake in subtropical coastal marshes. *Sci. Total Environ.* 747:141214. doi: 10.1016/j.scitotenv.2020.141214
- Li, Y., Long, C., Dai, Z., and Zhou, X. (2024). Pattern of total organic carbon in sediments within the mangrove ecosystem. *Front. Mar. Sci.* 11:1428229. doi: 10.3389/fmars.2024.1428229
- Liu, X., Xia, J., Wright, G., and Arnold, L. (2014). A state of the art review on high Water mark (HWM) determination. *Ocean Coast. Manage.* 102, 178–190. doi: 10.1016/j.ocecoaman.2014.09.027
- Lovelock, C. E., Cahoon, D. R., Friess, D. A., Guntenspergen, G. R., Krauss, K. W., Reef, R., et al. (2015). The vulnerability of Indo-Pacific mangrove forests to sea-level rise. *Nature* 526, 559–563. doi: 10.1038/nature15538
- Lovelock, C. E., Feller, I. C., Reef, R., Hickey, S., and Ball, M. C. (2017). Mangrove dieback during fluctuating sea levels. *Sci. Rep.* 7:1680. doi: 10.1038/s41598-017-01927-6
- Lovelock, C. E., Krauss, K. W., Osland, M. J., Reef, R., and Ball, M. C. (2016). “The physiology of mangrove trees with changing climate” in *Tropical tree physiology: Adaptations and responses in a changing environment*, eds G. Goldstein and L. S. Santiago (Cham: Springer International Publishing), 149–179.
- Lu, W., Xiao, J., Liu, F., Zhang, Y., Liu, C., and Lin, G. (2017). Contrasting ecosystem CO₂ fluxes of inland and coastal wetlands: a meta-analysis of eddy covariance data. *Glob. Chang. Biol.* 23, 1180–1198. doi: 10.1111/gcb.13424
- Maiti, S. K., and Chowdhury, A. (2013). Effects of anthropogenic pollution on mangrove biodiversity: a review. *J. Environ. Prot.* 4, 1428–1434. doi: 10.4236/jep.2013.412163
- Masouleh, Z. P. (2015). Identification of sea breezes, their climatic trends and causation, with application to the Adelaide coast thesis, School of Civil, environmental and mining engineering. Adelaide: The University of Adelaide.
- Mauder, M., Cuntz, M., Drüe, C., Graf, A., Rebmann, C., Schmid, H. P., et al. (2013). A strategy for quality and uncertainty assessment of long-term eddy-covariance measurements. *Agric. For. Meteorol.* 169, 122–135. doi: 10.1016/j.agrformet.2012.09.006
- Miller, S. T. K., Keim, B. D., Talbot, R. W., and Mao, H. (2003). Sea breeze: structure, forecasting, and impacts. *Rev. Geophys.* 41:1–31. doi: 10.1029/2003rg000124
- Montgomery, J. M., Bryan, K. R., Mullarney, J. C., and Horstman, E. M. (2019). Attenuation of storm surges by coastal mangroves. *Geophys. Res. Lett.* 46, 2680–2689. doi: 10.1029/2018gl081636
- Moore, R., Miller, P., Ehleringer, J., and Laurence, W. 1973 Seasonal trends in gas exchange characteristics of three mangrove species. *Photosynthetica*, 7, 387–394.
- Morris, J. T., Sundareshwar, P. V., Nietch, C. T., Kjerfve, B., and Cahoon, D. R. (2002). Responses of coastal wetlands to rising sea level. *Ecology* 83, 2869–2877. doi: 10.1890/0012-9658(2002)083[2869:Rocwtr]2.0.CO;2
- Morrisey, D., Swales, A., Dittmann, S., Morrison, M., Lovelock, C., and Beard, C. (2010). The ecology and management of temperate mangroves. *Oceanogr. Mar. Biol.* 48, 43–160. doi: 10.1201/EBK1439821169-c2
- Narayan, S., Thomas, C., Matthewman, J., Shepard, C., Geselbracht, L., Nzerem, K., et al. (2019). Valuing the flood risk reduction benefits of Florida’s mangroves. *The Nature Conservancy*. Arlington.
- Noor, T., Batool, N., Mazhar, R., and Ilyas, N. (2015). Effects of siltation, temperature and salinity on mangrove plants. *Eur. Acad. Res.* 2, 14172–14179.
- Okazak, S. 2024 Piecewise linear model. In MATLAB central file exchange. Available online at: <https://www.mathworks.com/matlabcentral/fileexchange/124190-piecewise-linear-model> (accessed [01 06, 2026]).
- Papanastasiou, D. K., Melas, D., Bartzanas, T., and Kittas, C. (2010). Temperature, comfort and pollution levels during heat waves and the role of sea breeze. *Int. J. Biometeorol.* 54, 307–317. doi: 10.1007/s00484-009-0281-9
- Paramita Nandy, P. N., Sauren Das, S. D., Groom, P., Kabanoff, E., Monoranjan Ghose, M. G., and Spooner-Hart, R. (2007). On the physiological responses of *Avicennia marina* (Forsk.) Vierh. From Sydney, Australia in different salinity conditions. *Res. J. Bot.* 2, 33–40.
- Parida, A. K., and Jha, B. (2010). Salt tolerance mechanisms in mangroves: a review. *Trees* 24, 199–217. doi: 10.1007/s00468-010-0417-x
- Perkins-Kirkpatrick, S., and Lewis, S. (2020). Increasing trends in regional heatwaves. *Nat. Commun.* 11:3357. doi: 10.1038/s41467-020-16970-7
- Perri, S., Detto, M., Porporato, A., and Molini, A. (2023). Salinity-induced limits to mangrove canopy height. *Glob. Ecol. Biogeogr.* 32, 1561–1574. doi: 10.1111/geb.13720
- Pezeshki, S. R. (2001). Wetland plant responses to soil flooding. *Environ. Exp. Bot.* 46, 299–312. doi: 10.1016/S0098-8472(01)00107-1
- Radabaugh, K. R., Dontis, E. E., Chappel, A. R., Russo, C. E., and Moyer, R. P. (2021). Early indicators of stress in mangrove forests with altered hydrology in Tampa Bay, Florida, USA. *Estuar. Coast. Shelf Sci.* 254:107324. doi: 10.1016/j.ecss.2021.107324
- Reef, R., Slot, M., Motro, U., Motro, M., Motro, Y., Adame, M. F., et al. (2016). The effects of CO₂ and nutrient fertilisation on the growth and temperature response of the mangrove *Avicennia germinans*. *Photosynth. Res.* 129, 159–170. doi: 10.1007/s11120-016-0278-2
- Reichstein, M., Falge, E., Baldocchi, D., Papale, D., Aubinet, M., Berbigier, P., et al. (2005). On the separation of net ecosystem exchange into assimilation and ecosystem respiration: review and improved algorithm. *Glob. Change Biol.* 11, 1424–1439. doi: 10.1111/j.1365-2486.2005.001002.x
- Rhoades, J. (1990). Determining soil salinity from measurements of electrical conductivity. *Commun. Soil Sci. Plant Anal.* 21, 1887–1926. doi: 10.1080/00103629009368347
- Rhoades, J., Kandish, A., and Mashali, A. M. (1992). “The use of saline waters for crop production” in *FAO irrigation and drainage paper*, vol. 48, 133.
- Richards, D. R., Thompson, B. S., and Wijedasa, L. (2020). Quantifying net loss of global mangrove carbon stocks from 20 years of land cover change. *Nat. Commun.* 11:4260. doi: 10.1038/s41467-020-18118-z
- Ross, M. S., Ruiz, P. L., Sah, J. P., and Hanan, E. J. (2009). Chilling damage in a changing climate in coastal landscapes of the subtropical zone: a case study from South Florida. *Glob. Change Biol.* 15, 1817–1832. doi: 10.1111/j.1365-2486.2009.01900.x
- Saintilan, N., Wilson, N. C., Rogers, K., Rajkaran, A., and Krauss, K. W. (2014). Mangrove expansion and salt marsh decline at mangrove poleward limits. *Glob. Chang. Biol.* 20, 147–157. doi: 10.1111/gcb.12341
- Sanders, C. J., Eyre, B. D., Santos, I. R., Machado, W., Luiz-Silva, W., Smoak, J. M., et al. (2014). Elevated rates of organic carbon, nitrogen, and phosphorus accumulation in a highly impacted mangrove wetland. *Geophys. Res. Lett.* 41, 2475–2480. doi: 10.1002/2014GL059789
- Schreiber, J. B., Nora, A., Stage, F. K., Barlow, E. A., and King, J. (2010). Reporting structural equation Modeling and confirmatory factor analysis results: a review. *J. Educ. Res.* 99, 323–338. doi: 10.3200/joer.99.6.323-338
- Senger, D. F., Saavedra Hortua, D. A., Engel, S., Schnurawa, M., Moosdorf, N., and Gillis, L. G. (2021). Impacts of wetland dieback on carbon dynamics: a comparison

- between intact and degraded mangroves. *Sci. Total Environ.* 753:141817. doi: 10.1016/j.scitotenv.2020.141817
- Sippo, J. Z., Lovelock, C. E., Santos, I. R., Sanders, C. J., and Maher, D. T. (2018). Mangrove mortality in a changing climate: an overview. *Estuar. Coast. Shelf Sci.* 215, 241–249. doi: 10.1016/j.ecss.2018.10.011
- Smith, T. J., Anderson, G. H., Balentine, K., Tiling, G., Ward, G. A., and Whelan, K. R. (2009). Cumulative impacts of hurricanes on Florida mangrove ecosystems: sediment deposition, storm surges and vegetation. *Wetlands* 29, 24–34. doi: 10.1672/08-40.1
- Song, S., Ding, Y., Li, W., Meng, Y., Zhou, J., Gou, R., et al. (2023). Mangrove reforestation provides greater blue carbon benefit than afforestation for mitigating global climate change. *Nat. Commun.* 14:756. doi: 10.1038/s41467-023-36477-1
- Stong, M. (2008). Development of remote sensing techniques for assessment of salinity induced plant stresses: Tucson. The University of Arizona.
- Torres, R., Snoeij, P., Geudtner, D., Bibby, D., Davidson, M., Attema, E., et al. (2012). GMES sentinel-1 mission. *Remote Sens. Environ.* 120, 9–24. doi: 10.1016/j.rse.2011.05.028
- Water, D. F. E. A. (2021). Dry Creek salt fields vegetation impact mapping. DEW technical report 2021/14.
- Webb, E. K., Pearman, G. I., and Leuning, R. (1980). Correction of flux measurements for density effects due to heat and water-vapor transfer. *Q. J. R. Meteorol. Soc.* 106, 85–100. doi: 10.1002/qj.49710644707
- Whittaker, T. A. (2012). Using the modification index and standardized expected parameter change for model modification. *J. Exp. Educ.* 80, 26–44. doi: 10.1080/00220973.2010.531299
- Wilczak, J. M., Oncley, S. P., and Stage, S. A. (2001). Sonic anemometer tilt correction algorithms. *Boundary-Layer Meteorol.* 99, 127–150. doi: 10.1023/A:1018966204465
- Wutzler, T., Lucas-Moffat, A., Migliavacca, M., Knauer, J., Sickel, K., Šigut, L., et al. (2018). Basic and extensible post-processing of eddy covariance flux data with REddyProc. *Biogeosciences* 15, 5015–5030. doi: 10.5194/bg-15-5015-2018
- Xiong, Y., Dai, Z., Long, C., Liang, X., Lou, Y., Mei, X., et al. (2024). Machine learning-based examination of recent mangrove forest changes in the western Irrawaddy River Delta, Southeast Asia. *Catena* 234:107601. doi: 10.1016/j.catena.2023.107601
- Zhang, Z., Luo, X., Friess, D. A., Wang, S., Li, Y., and Li, Y. (2024). Stronger increases but greater variability in global mangrove productivity compared to that of adjacent terrestrial forests. *Nat. Ecol. Evol.* 8, 239–250. doi: 10.1038/s41559-023-02264-w
- Zhou, Y., Guan, H., Gharib, S., Batelaan, O., and Simmons, C. T. (2021). Cooling power of sea breezes and its inland penetration in dry-summer Adelaide, Australia. *Atmos. Res.* 250:105409. doi: 10.1016/j.atmosres.2020.105409
- Zhu, X., Qin, Z., and Song, L. (2021). How Land-Sea interaction of tidal and sea breeze activity affect mangrove net ecosystem exchange? *J. Geophys. Res. Atmos.* 126:e2020JD034047. doi: 10.1029/2020jd034047